Gully erosion in Northeast China – a case study on history, erosion rates and causes

Yanru Wen[1,2], Till Kasielke[3], Hao Li[4], Harald Zepp[3], Bin Zhang[1]*

[1] *Institute of Agricultural Resources and Regional Planning, Chinese Academy of Agricultural Sciences, Beijing, 100081, PR China.*

[2] *Key Laboratory of Agricultural Remote Sensing (AGRIRS), Beijing, 100081, PR China.*

[3] *Department of Geography, Ruhr University Bochum, Universitätsstr.150, 44780 Bochum, Germany.*

[4] *Northeast Institute of Geography and Agroecology, Chinese Academy of Sciences, Harbin, 150081, PR China.*

*Corresponding author:

B Zhang, E-mail: zhangbin01@caas.cn. Tel/Fax: +86 10 82105635

Manuscript submitted to: Land Degradation & Development

Submission date: 4 February, 20214

Graphical abstract

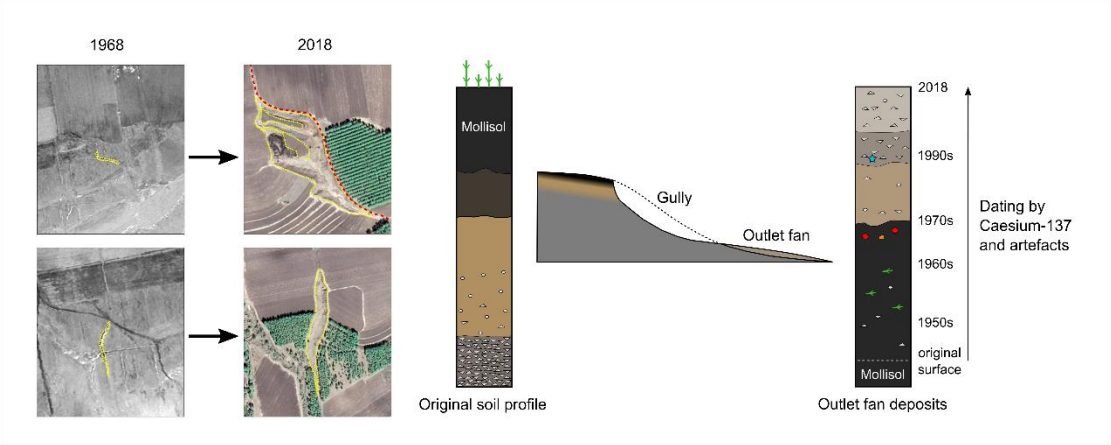

Highlights

- Gully erosion history in a typical village was estimated by gully morphology and radioisotope
- Gully erosion started in 1950-60s due to large-scale agricultural extension in Northeast China
- Gullies were initiated on steeper slopes with shallowly buried shales and along unpaved roads
- Gully head retreated by 1.5 to 2.5 m yr^{-1} and soil loss from gullies ranged from 25.7 to 44.7 Mg yr^{-1} ha^{-1}

Abstract

Mollisols are of major importance for food security worldwide but are increasingly degraded by soil erosion. Mollisols in Northeast China have been converted into agricultural use only recently, but gullies are widely distributed and gully erosion history, rates and causes remained unclear. We chose a study typical village to estimate initiation years and development rates of the gully systems from 1968 to 2018 by using aerial and satellite imagery. The outlet fan deposits of a large gully system were dated by Caesium-137 (^{137}Cs) and artefacts. To verify the results, we collected information from local farmers. Gully volumes were measured by structure-from-motion technique using photos taken from an unmanned aerial vehicle. Our results showed that gully systems had already appeared on the steep slopes and along unpaved roads in 1968 and had become more complex by 2018 despite terracing and afforestation. Based on gully morphology and ^{137}Cs, gully erosion was estimated to have started in the 1950s to 1960s when the original grassland and forest were completely converted into arable land. From 1968 to 2018, the gully density increased from 1.2 to 2.3 km km^{-2}. The gully heads retreated at speeds from 1.5 to 2.5 m yr^{-1}, and the soil loss from gully erosion ranged from 25.7 to 44.7 Mg yr^{-1} ha^{-1}. These data demonstrate the severity of gully erosion in the study region and underline the importance of appropriate countermeasures, such as maintenance of abandoned terraces under reforested land and better design and construction of roads within the arable lands.

Keywords: Gully erosion; Erosion rate; Remote sensing; ^{137}Cs; Mollisol

1. Introduction

Mollisols cover ~7% of the global ice-free land area. They are the most important soil order for food production because of their deep surface horizons with a high content of soil organic carbon. Mollisols are severely threatened by soil degradation under improper soil management as they have globally been converted from native forest or steppe/grassland into arable lands since the 19th century (Liu et al., 2012). In Northeast China, Mollisols have been used for agriculture on a large scale since the 1950s (Ye & Fang, 2011). The Mollisol region has become the largest granary in China since the late 1990s, contributing to the annual food demand of more than 216 million urban citizens (Liu et al., 2011). However, more than 290,000 active gullies have been reported in the Mollisol region, posing a big threat to local soil quality and national food security (Liu & Yan, 2009; Ministry of Water Resources et al., 2010). It remains unclear why, when, and how fast gullies have developed in Northeast China. This knowledge is crucial for decision makers and farmers to take proper and prompt measures in preventing further gully erosion in the region.

Gullies develop along drainage lines on slopes and the gully volumes become larger in different directions due to gully heads retreating backwards up the slope, sidewalls collapsing and down cutting (Aber et al., 2019; Harvey, 1992). Thus, gully expansion rates are often calculated by measuring the gully head retreat distance or changes in gully morphology and volume using GPS data or aerial photography over a defined period (Gudino-Elizondo et al., 2018; Marzolff & Poesen, 2009; Vandekerckhove et al., 2001). Yet, the use of airborne techniques is limited due to the lack of high-resolution aerial photos for older periods. Thus, the initiation time of gullies and long-term gully erosion rates are often unknown (Castillo & Gomez, 2016; Frankl et al., 2012; Poesen, 2018).

In addition to interviews with local farmers and experts (Frankl et al., 2011; Moges & Holden, 2008; Nyssen et al., 2006), the investigation of colluvial deposits can provide

insight into soil erosion history at a local scale (Dotterweich et al., 2003; Mieth & Bork, 2010; Kasielke & Zepp, 2011; Kasielke et al., 2019). Embedded and buried artefacts combined with scientific dating techniques often enable a direct linkage of settlement and land use with gully erosion events (Bork & Lang, 2003; Kappler et al., 2018; Vattuone et al., 2018). Radiocaesium-137 (^{137}Cs) has been widely used to estimate deposition rates since the 1960s (Porto & Walling, 2012; Zhang et al., 2017).

Previous studies on gully erosion in the Mollisol region of Northeast China were mostly based on short-term monitoring, often focusing on ephemeral gullies (Hu et al. 2007; Zhang et al., 2007; Wu et al., 2008), while only little information is available on long-term erosion rates and the beginning of gully erosion in this region. The objectives of this study were to 1) characterize gully changes over a time interval of 50 years (1968 to 2018) in an agricultural area representative of the Mollisol region in Northeast China, 2) estimate initiation years and erosion rates, and 3) understand the gully erosion processes and driving forces in the region.

2. Materials and Methods

2.1. Study area

Our study area (20 km²) is located in Guangrong village, about 15 km southwest of Hailun city, Heilongjing Province of China (47°21'N, 126°45'E). This region has a temperate continental monsoon climate. The mean annual temperature is 1.5 ℃, with the highest mean monthly temperature of 21.7 ºC in July and lowest in January (-21.8 ℃). The frost season lasts from late October to late April. The mean annual precipitation is 543 mm, about 78% of which is distributed from June to September. Over the last 58 years, since a weather station was established, there were 32 storm events with a rainfall intensity > 50 mm d^{-1} and two with recorded rainfall as high as 85.3 and 112.7 mm d^{-1} in June of 1966 and 1975,

103 respectively. The regional soil was classified as a Typic Hapludoll according to USDA Soil
104 Taxonomy (Soil Survey Staff, 2010), corresponding to Haplic Phaeozem in the FAO
105 classification (FAO, 2015). The mollic epipedon was up to 70 cm in depth and developed
106 in Pleistocene loess, which was underlain by fluvial sediments of varying grain size (silt,
107 sand, pebbles) and shale (Sun & Liu, 2001). The landforms in the study area were typical
108 for the region, exhibiting long (> 200 m) and gentle slopes.
109
110 ***2.2. Gully change between 1968 and 2018***
111 The earliest available aerial photograph from 16th September 1968 and a satellite image
112 from 19th July 2017 were collected for the studied area. The aerial photograph was available
113 from the Heilongjiang (Province) Bureau of Surveying and Mapping Geographic
114 Information, with a scale of 1:15,000 and a resolution of 0.6 m. The satellite image was
115 available from the Digital Globe of Google, with a resolution of 0.3 m. These images were
116 geo-referenced in a GIS environment using the UTM 52N coordinate system. Correct
117 positions were checked in the field using differential GPS in early April 2018. We derived
118 a Digital Elevation Model (DEM) for the study area by digitizing the contour lines from a
119 topographical map from 1982 (scale 1:10,000) and transformed into a raster of 1.0 m
120 resolution. Based on the spatial dataset, we mapped land use, unpaved field cart roads and
121 gully systems for 1968 and 2018 (Fig. 1). During field mapping, the gullies featuring lack
122 of vegetation cover on the gully walls and fresh sediments on the gully floor were marked
123 as active gullies. All other gullies were marked as inactive.
124 Based on the DEM, the study area was subdivided into 20 catchments (Fig. 1b). Small
125 gully catchments were merged with adjacent ones to avoid their number becoming too large.
126 We determined total gully length by measuring the lengths of all gullies including their side
127 gullies for 1968 and 2018. The main gully was defined as the one that connected the outlet

and the uppermost gully head. If a catchment included several independent gullies, we took only the longest gully in 2018 to measure the main gully length. The gully density of each catchment was calculated as the total gully length divided by the drainage area.

2.3 Measurements of gully volume and erosion rates

Gullies A–D (Fig. 1), which had already appeared on the aerial photo of 1968, were used to determine gully area, gully volume and rates of gully head retreat. Gully volume was measured in April 2018 by structure-from-motion technique using photos taken an unmanned aerial vehicle (UAV) (DJI Phantom 4, Shen Zhen DJI Technology Co., Ltd). At that time, the gully floors were neither covered by snow nor by growing plants so that there was a minimum impact of vegetation. The digital camera captured one image per second from 50 m above the ground and was mounted facing 15% from vertical to avoid doming deformations. Structure-from-motion techniques were used to create a Digital Surface Model (DSM) and an orthophoto of the targeted gully system from a series of non-calibrated images based on sixteen ground control points distributed within the whole gully and its surroundings. Elevation and position of the ground control points were measured using a differential GPS (Galaxy G6 RTK system, South Surveying) with a vertical accuracy of 8 mm. The DSM with a 0.3 m spatial resolution and the orthophoto with a 0.04 m spatial resolution were generated using Pix4D mapper software (Pix4d, Lausanne, Switzerland) and geo-referenced using ArcGIS software. The gully boundary was then estimated using the DSM and the orthophoto. The gully volume was determined by comparing the DSM with the original slope surface before the gully development using the cut-fill spatial analysis tool of the ArcGIS environment.

We calculated the average soil loss rate per catchment area (Mg yr^{-1} ha^{-1}) according to Tebebu et al. (2010) (Eq. 1).

$$R = \frac{V * Bd}{T * A} \quad (1)$$

where, R is the yearly soil loss rate per catchment area; V is the gully volume (m^3); Bd is the average soil bulk density of 1.27 g cm^{-3}, measured with metal cylinders at depths of 0-10, 10-20, 20-40, 40-60 and 60-100 cm; T is the number of years covering the formation of a gully; and A is the gully catchment (ha) of the gully system.

The initiation years of the selected gullies was estimated based on its area in 1968 and its extension rate estimated between 1968 and 2018 according to Nyssen et al., 2006 (Eq. 2).

$$T_1 = T_2 - \frac{A}{R_A} \quad (2)$$

where, T_1 is the gully initiation year; T_2 is the year of 2018; A is the gully area in 1968 (m^2); R_A is the area extension rate (m^2 yr^{-1}) defined as the difference in the gully area between 2018 and 1968 divided by 50 years. The calculated initiation years were checked and confirmed by interviews with local farmers.

2.4. Gully outlet fan deposits and ^{137}Cs measurement

Within a 250 m-long trench at the outlet fan of Gully A, thirteen soil profiles were described in detail to characterize the deposits and determine where to take samples. Soil texture of each layer was estimated by finger test (texture classes according to FAO, 2006). Three profiles were sampled in 5 cm intervals to determine the vertical distribution of ^{137}Cs. In addition, an old (> 80 years) forest on a flat topography was selected as a reference site without soil erosion to measure the ^{137}Cs activity. ^{137}Cs is an artificial radionuclide (half-life: 30.2 years) produced by nuclear weapons testing (Sutherland, 1989; Walling & Quine, 1990), especially in the 1960s. Fallout ^{137}Cs is rapidly absorbed to the fine fraction of surficial soils and eventually redistributed by erosion (Owens et al. 1997). The soil samples were air-dried and passed through a 2 mm sieve for the measurement of radioisotope concentration using an ORTEC spectrometer with an HPGe detector of GWL-120-15

178 (AMETEL-AMT ORTEC Co.) The samples were detected at 662 keV peak with a counting
179 time over 80,000 s, providing a measurement precision of ±5% for ^{137}Cs at the 95%
180 confidence level (Fang et al., 2012).
181
182 **3. Results**
183 ***3.1. Gully pattern development between 1968 and 2018***
184 Most of the gully systems had already appeared in 1968 (Fig. 1). The highest gully density
185 in both years was found where the terrain was steepest, with slopes ranging from 5% to 11%.
186 Gullies A–C had been retreating upwards into the hilltops since 1968 along unpaved field
187 cart roads, or paths made by pedestrians and cattle (Fig. 2).
188 Compared to 1968, the gully systems had become more complex with the development
189 of side gullies until 2018 (Fig. 1). The total gully length increased from 24.0 to 46.7 km and
190 total gully density from 1.2 to 2.3 between 1968 and 2018. In 2018, the gully densities in
191 the 20 catchments ranged from 0.9 to 6.0 km km^{-2}, with fifteen of which having a gully
192 density ≥2.0 km km^{-2}. About 90% of the total gully length in 2018 was actively eroding.
193 Even under forest, 82% of 23.5 km were active (Table 1).
194
195 ***3.2. Gully initiation years and erosion rates***
196 Based on the gully dimensions in 1968 and the extension rate between 1968 and 2018, we
197 calculated initiation years between 1955 and 1966 for the Gullies A–D, which is consistent
198 with the onset of gully development reported by the local farmers (Table 2). The oldest and
199 largest Gully A (Fig. 3a) had a catchment area of 43.9 ha and a volume of 93,780 m^3 in 2018,
200 giving a mean soil loss rate in the catchment area of 42.4 Mg yr^{-1} ha^{-1}. For the other three
201 Gullies B–D with catchment areas between 5.4 and 12.7 ha and volumes between 7,630 and
202 17,045 m^3 the yearly soil loss ranged from 25.7 to 44.7 Mg yr^{-1} ha^{-1}. The gully head retreat

rates of the four gullies ranged from 1.5 to 2.5 m yr^{-1} and the gully area increased by 57 to 165 m^2 yr^{-1} (Table 2).

3.3 Soil profiles at the gully outlet fan

Figure 4a shows the soil profiles along the trench at the outlet fan of Gully A (Fig. 4b). The colors of the soil columns resemble the colors of the fresh soil. For orientation, the same coloring is used in the reference profile (Fig. 4c). Black colors stand for black material, rich in organic matter, whose color is comparable to the mollic epipedon of non-eroded solid of the study area. The lighter the colors, the lower the organic content, as in the reference profile.

Profile P1 started with black silty clay at the bottom below 80 cm, turning into dark greyish brown between 65 and 80 cm. A high ^{137}Cs activity was detected at a depth of 75 to 95 cm (Fig. 5). The upper 65 cm of the profile was stratified, and soil colors ranged from darker brownish grey to pale yellowish brown. At a depth of 42 cm, we found plastic material from a detergent container. Profile P2 generally resembled P1. Again, plastic material appeared at about 60 cm. We encountered some shale fragments and pebbles right on top of the black material. Profiles P3 and P4 contained brownish silty clay free of coarse fragments, underlain by black material in P4.

Profiles P5 to P13 possessed intercalated layers containing coarse fragments. In P5, in common with P7, the black material is underlain by brownish material. The upper boundaries of the two lowermost layers of P5 below the black material were bent, which is unlikely for horizon boundaries in Mollisols. Furthermore, the second lowermost layer showed an alternation of thin layers with variable content of organic matter, proving its colluvial origin. Hence, the overlying black material was also a colluvial deposit. In the middle layer of P6, undecayed grass remains and alternating thin beds of different color indicate the colluvial nature. In profile P7 we found slag, coal, coke ash, and brick fragments between 95 and 120

cm as well as undecayed grass remains. The underlying silty clay layers contained pebbles and shale (Fig. 4). Between 75 and 115 cm ^{137}Cs could be detected in every sample and the activity partly reached high values of more than 5 Bq kg^{-1} (Fig. 5). Varying contents of coarse material occurred in the first 60 cm and below 140 cm. Profile P8 is made up of a matrix with varying colors and full of shale fragments down to 120 cm, underlain by black silty clay. The upper parts of P9 and P10 revealed brownish laminated fines with shale fragments. In P9, lenses and laminae of pale soil within the lowermost black layer indicated its colluvial origin. The black layers in P11 and P12 were remarkably thick, being 100 and 80 cm, respectively. Profile P11 had several striking features: The greyish-black fine soil overlaid brownish silty clay with a sharp boundary, dipping from 140 to 205 cm. Both layers contained well preserved remnants of horsetail (*Equisetum*) stems, indicating a young colluvial origin. Above an intermediate layer, we found fine-layered silt loam between 75 and 92 cm. The top layers had varying textures and colors and contain shale particles (Fig. 4). Continuous ^{137}Cs activity was measured between 95 and 140 cm, with a maximum at 100 cm (Fig. 5). Profile P13 started with a black layer, exposed between 75 and 120 cm, which was overlain by a brownish-grey soil material. Above it, all layers contained shale fragments, and at a depth of 40 cm, we encountered a brick fragment (Fig. 4).

4. Discussion

4.1. Gully erosion history

The analysis of the aerial photo of 1968 (Fig. 1a) demonstrated that gully erosion was already severe in the study area in the 1960s. Based on the gully area and gully extension rate, we calculated that the gullies initiated in the mid-1950s and 1960s. Although the dating implies a constant rate of gully extension, the results agree with the times of gully initiation

252 reported by local farmers (Table 2) and the onset of large-scale arable farming in the study
253 area.

254 The soil profiles at the outlet fan of Gully A allowed for a more detailed reconstruction
255 of the erosion history of this specific gully. Most of the material exposed in the profiles was
256 undoubtedly of colluvial origin as evidenced by coarse fragments (shale and pebbles within
257 a matrix of fines), high ^{137}Cs activity at greater depth, embedded artefacts, and plant remnants
258 (Fig. 4; Fig. 5). Prior to soil erosion, the whole study area was covered by Pleistocene loess,
259 on which Mollisols had developed (Fig. 4c). In the profiles at the outlet fan, a clear distinction
260 between the original Mollisol and the black colluvial layer with a high organic content was
261 not always possible in profiles with black bottom layers. However, in many profiles we found
262 clear indications that black sediment derived from the mollic epipedon has been deposited on
263 the fan in the early phase of colluviation. The general sequence of inverted soil profiles is
264 visible in most of the profiles, where the sediments become less dark (i.e. the content of
265 organic carbon decreases) and the content of coarse fragments increases toward the top (Fig.
266 4).

267 ^{137}Cs-analyses in the profiles P2, P7 and P11 (Fig. 5) allowed for a rough dating of the
268 sediments. The deepest occurrence of ^{137}Cs can be equated with the onset of ^{137}Cs in the
269 1950s, although a small proportion may have migrated down the profile. High ^{137}Cs
270 concentrations are likely to indicate colluvial sediments from the 1960s, when nuclear fallout
271 reached its maximum (Owens et al., 1997). However, we must consider that the initial spatial
272 distribution of ^{137}Cs was not uniform on a large scale (Parsons & Foster, 2011; Zhang, 2015;
273 Zhang et al., 2019a). Furthermore, the ^{137}Cs depth profiles reflect both direct fallout from the
274 atmosphere and delayed input of ^{137}Cs-enriched colluvial sediments from the gully catchment.
275 As the timespan between fallout on the soil surface in the catchment and deposition on the
276 outlet fan is unknown, only rough estimations of the time of deposition can be made.

In profile P1, located in the most distal part of the fan, we found faint structural hints that the original mollic epipedon began at 85 cm depth. The high ^{137}Cs activity between 85 and 95 cm therefore probably reflects direct fallout on the fan. As ^{137}Cs was rapidly absorbed to the fine fraction of the soil and retained in the top few centimeters (Owens et al., 1997), the ^{137}Cs activity dropped sharply in 95-100 cm. The high ^{137}Cs concentrations at 75-85 cm suggest a deposition during the 1960s. The three samples above 75 cm were virtually free from ^{137}Cs and had lighter soil color. These results can be explained by erosion of subsoil material in the gully and subsequent deposition on the fan. The plastic found at 42 cm was recognized as the package of a detergent produced not earlier than 1992. The agricultural plastic foil in profile P2 (60 cm depth) was introduced from Japan not earlier than 1979 (Chen, 2014). These modern artefacts prove that gully erosion continued after large parts of the catchment had been terraced between 1968 and 1974 (Wen et al., 2021).

In profile P7, charcoal, slag, and hard coal particles probably derived from a small brick kiln factory and a small iron boiler established between 1967 and 1970 near the head of the gully. This is in line with high and continuous ^{137}Cs activity between 75 and 130 cm, which can be attributed to the 1960s. Notable ^{137}Cs concentrations could also be detected in most of the samples below down to the lowermost sample in 200-205 cm. It is unlikely that this was caused by post-depositional downward migration in the profile because this would create a rather constant decline of ^{137}Cs with increasing depth. The colluvial origin of the whole profile is further indicated by numerous shale fragments and some pebbles in the lowermost sediments (>140 cm depth). This, in turn, suggests that a gully had existed when the sediments were deposited. Otherwise, it would not have been possible to deliver shale and pebbles to the outlet fan. We conclude that the lower part of P7 is a colluvial sediment from the 1950s, while the sediments with higher ^{137}Cs concentrations between ca. 60 and 130 cm were

deposited from the 1960s onward. The upper sediments mainly result from erosion of subsoil and shale in the gully.

Profile P11 is located at the most proximal position of the outlet fan and therefore probably received the earliest colluvial deposits. The well-preserved horsetail stems found in the two lowermost layers indicate a young colluvial origin of the whole profile. Considerable amounts of ^{137}Cs were detected between 95 and 130 cm, suggesting a deposition between ca. 1955 and 1970. The pronounced peak at 95-105 cm might be equated with the fallout peaks around 1963. The upper 85 cm of P11 are virtually free from ^{137}Cs. As in P7, these sediments derive from subsoil and shale eroded in the gully.

To summarize, we conclude that Gully A already existed prior to the 1960s. However, until the 1960s, erosion mostly affected the deep mollic surface horizons in the catchment. From then on, the outlet fan deposits reflect a rapid extension and downcutting of the gully that continued up to the present despite terracing and afforestation in parts of the catchment (Fig. 3a).

4.2. Gully erosion rates and driving forces

The mean gully density in the study area is 2.3 km km^{-2} (Table 1). Gully densities in the same order of magnitude have been observed in other parts of the Mollisol region of Northeast China (Xu et al., 2014; Yang et al., 2017; Liu et al., 2020). 4.3 km km^{-2} have been reported from the upper reaches of Yangtze River, Southwest China, and 5.9 km km^{-2} from the Loess Plateau, Northwest China (Liu et al., 2013; Xu et al., 2018). The gully head retreat rates of 1.5 to 2.5 m yr^{-1} in our study area (Table 2) are lower than mean head retreat rates obtained elsewhere in the Mollisol region of Northeast China (6.2 m yr^{-1}, Hu et al., 2007; 8.4 m yr^{-1}, Wu et al., 2008). However, the soil loss rates from our studied gullies (Table 2) were much higher than previously reported from the Mollisol region of Northeast China (10.1 Mg ha^{-1}

yr^{-1}, Wu et al., 2008; 4.5 Mg ha^{-1} yr^{-1}, An et al., 2014). Lower head retreat rates but higher soil loss in our study can be explained by the smaller size and younger age of the gullies studied by Wu et al. (2008). Soil loss is not only related to head retreat, but also controlled by gully incision, side gully development, and erosion of the gully banks and therefore by gully length. Furthermore, it can be assumed that the head retreat rates of Gullies A–D were higher in the early stage of their development due to larger areas draining to the gully heads.

In China, the southwestern and northwestern regions are most famous for gully erosion before the 1990s and for effective soil erosion control after the campaign of "Grain for Green" since the 2000s (Cao et al., 2009; Li et al., 2020; Zhao et al., 2013). The soil loss rates obtained from our study area are as high as those in the Loess Plateau of Northwest China (18.8 to 43.0 Mg ha^{-1} yr^{-1}; Poesen et al., 2003), but lower than in the Dry-hot valley region of Southwest China (164 Mg ha^{-1} yr^{-1}, Yang et al., 2015). Compared to the southwestern and northwestern regions of China, precipitation is lower, slopes are gentler, and soils are richer in organic carbon in the Mollisol region of Northeast China. However, gully extension rates and soil loss rates by gullying are high and terracing and reforestation did not successfully control gully erosion as reported in many other regions of China.

There are several reasons for this. Firstly, despite its high organic carbon content, surface soils are generally cohesionless and structurally weak. Freezing and thawing cycles result in soil bulk densities being even lower than 1.0 Mg m^{-3} after winter and increase to more than 1.4 Mg m^{-3} after soil compaction. Secondly, the Mollisols in our study area developed from loess with a high clay content, which makes the soil impermeable particularly after compaction. This causes large amounts of overland flow which is concentrated at the lower slope position after snowmelt in spring and rainstorms in summer and thereby initiate gully development. Depending on the shear stress and scouring force of the overland flow, gully heads retreat quickly during these periods (Hu et al., 2007). Thirdly, the loess-derived parent

material of the Mollisols and underlying fluvial sediments and shales (Fig. 4c) have less cohesion than the surface mollic soil layers. Once the cohesionless shales are exposed, for example, at the edge of the steep slopes along the Hailun River plain (Fig. 1; Fig. 3b), gully development is accelerated through gully-wall collapse by gravity and gully-floor incision. Collapse of these materials may accelerate the slumping of the mollic surface soil even if plant roots stabilize the soil (Barnes et al., 2016; Vanmaercke et al., 2016).

Heavily dissected badland landscapes in the Mediterranean have also been attributed to specific lithologic conditions, i.e. the presence of unconsolidated or poorly sorted materials such as shales and silt-clay deposits of Quaternary age (Poesen et al., 2003). In addition, frequent and intensive freezing and thawing in winter may further contribute to the destabilization of gully walls (Collison, 2001; Ma et al., 2019; Xu et al., 2019). Moreover, the compacted unpaved field cart roads concentrate overland flow and increase shear stress and scouring force along the roads, accelerating gully development once the less cohesive layers below the Mollisol are exposed. This was obvious in case of Gully C (Fig. 2), which is composed of two parallel straight gully segments in its lower section (Fig. 3b). The western segment developed first, probably caused by concentrated runoff along a former field cart road as suggested by the aerial photo from 1968 (Fig. 3a). In addition, the road in 1968 ran only a few meters away from this gully. Erosion along this road caused incision of the second gully, which was still active in 2018 (Fig. 3b). Gully erosion along unpaved roads has also been reported from China´s Loess Plateau (Zhang et al., 2019b). Moreover, poorly designed terraces and a lack of their maintenance (Arnáez et al., 2015; Tarolli et al., 2014) on the forested slopes enabled ongoing erosion and even induced the formation of new gullies in our study area (Wen et al., 2021).

4. Conclusions

This study demonstrated that gully erosion started in the 1950s when the original grasslands and shrub forests were converted into arable land on a large scale in the Mollisol region of Northeast China. Most gully systems initiated on steeper slopes where unconsolidated sediments and cohesionless shales lie close to the surface. Gully erosion accelerated during the 1960s and continued up to the present despite afforestation and terracing. The mean gully density doubled from 1.2 km km^{-2} in 1968 to 2.3 km km^{-2} in 2018. Four gullies which have been studied in detail expanded at rates of 1.5 to 2.5 m yr^{-1} between 1968 and 2018, resulting in soil loss at rates of 25.7 to 44.7 Mg ha^{-1} yr^{-1}. The estimated gully erosion rates are comparably as high as, or even higher than, the reported data from many regions around the world well-known for heavy gully erosion. Our findings point out the severeness of gully erosion in the Mollisol region of Northeast China and highlight the need of taking prompt and proper countermeasures to retain surface runoff. Further measures, such as avoiding gully initiation at locations with a shallow Mollisols above cohesionless materials, in combination with reorganizing unpaved roads or construction of subsurface drainage along the roads may help to control further gully development.

Acknowledgements

This study was funded by the National Key Research and Development Program of China (No. 2017YFC0504202/GX18B028). Xu Jinzhong and Zhen Huaicai helped in field investigations.

Conflict of Interest or Acknowledgments

The authors declare no competing financial interests.

401

402 **Data Availability Statement**

403 More detail data is available upon request

404

405 **Authors credit**

406 Bin ZHANG: Study design; Yanru WEN, Bin ZHANG, Till KASIELKE and Harald

407 ZEPP: Profile sample collection in the field, data interpretation and paper drafting. Yanru

408 WEN and Hao LI: DEM and UAV survey.

409

410 **References**

411 Aber, J. S., Marzolff, I., Ries, J. B., & Aber, S. E. W. (2019). Gully-Erosion Monitoring. In
412 J. S. Aber, I. Marzolff, J. B. Ries, & S. E. W. Aber (Eds.), *Small-Format Aerial*
413 *Photography and UAS Imagery* (pp. 259-271). Amsterdam: Elsevier.

414 An, J., Zheng, F., & Wang, B. (2014). Using ^{137}Cs technique to investigate the spatial
415 distribution of erosion and deposition regimes for a small catchment in the black soil
416 region, Northeast China. *Catena, 123*, 243-251. doi:10.1016/j.catena.2014.08.009

417 Arnáez, J., Lana-Renault, N., Lasanta, T., Ruiz-Flaño, P., & Castroviejo, J. (2015). Effects
418 of farming terraces on hydrological and geomorphological processes. A review.
419 *Catena, 128*, 122-134. doi:10.1016/j.catena.2015.01.021

420 Barnes, N., Luffman, I., & Nandi, A. (2016). Gully erosion and freeze-thaw processes in
421 clay-rich soils, northeast Tennessee, USA. *GeoResJ, 9-12*, 67-76.
422 doi:10.1016/j.grj.2016.09.001

423 Bork, H. R., & Lang, A. (2003). Quantification of past soil erosion and land use / land cover
424 changes in Germany. In A. Lang, R. Dikau, & K. Hennrich (Eds.), *Long Term*
425 *Hillslope and Fluvial System Modelling* (pp. 231-239). Berlin, Heidelberg: Springer.

426 Cao, S. X., Chen, L., & Yu, X. X. (2009). Impact of China's Grain for Green Project on the
427 landscape of vulnerable arid and semi-arid agricultural regions: a case study in
428 northern Shaanxi Province. *Journal of Applied Ecology, 46*(3), 536-543.
429 doi:10.1111/j.1365-2664.2008.01605.x
430 Castillo, C., & Gomez, J. A. (2016). A century of gully erosion research: Urgency,
431 complexity and study approaches. *Earth-Science Reviews, 160*, 300-319.
432 doi:10.1016/j.earscirev.2016.07.009
433 Chen, D. S. (2014). Application Status and Development of Mulch Film in China.
434 *Sugarcane and Canesugar,* (4), 50-54 (In Chinese with English abstract).
435 Collison, A. J. C. (2001). The cycle of instability: stress release and fissure flow as controls
436 on gully head retreat. *Hydrological Processes, 15*(1), 3-12. doi:10.1002/hyp.150
437 Dotterweich, M., Schmitt, A., Schmidtchen, G., & Bork, H. R. (2003). Quantifying
438 historical gully erosion in northern Bavaria. *Catena, 50*(2-4), 135-150.
439 doi:10.1016/S0341-8162(02)00142-X
440 Fang, H. Y., Sun, L. Y., Qi, D. L., & Cai, Q. G. (2012). Using ^{137}Cs technique to quantify
441 soil erosion and deposition rates in an agricultural catchment in the black soil region,
442 Northeast China. *Geomorphology, 169-170*, 142-150.
443 doi:10.1016/j.geomorph.2012.04.019
444 FAO (Food and Agriculture Organization of the United Nations). (2006). Guidelines for
445 soil description. 4th edition. Rome.
446 FAO (Food and Agriculture Organization of the United Nations). (2015). World reference
447 base for soil resources 2014. International soil classification system for naming soils
448 and creating legends for soil maps. Update 2015. World Soil Resources Reports 106.
449 Rome.

Frankl, A., Nyssen, J., De Dapper, M., Haile, M., Billi, P., Munro, R. N., Deckers, J., & Poesen, J. (2011). Linking long-term gully and river channel dynamics to environmental change using repeat photography (Northern Ethiopia). *Geomorphology, 129*(3-4), 238-251. doi:10.1016/j.geomorph.2011.02.018

Frankl, A., Poesen, J., Deckers, J., Haile, M., & Nyssen, J. (2012). Gully head retreat rates in the semi-arid highlands of Northern Ethiopia. *Geomorphology, 173*, 185-195. doi:10.1016/j.geomorph.2012.06.011

Gudino-Elizondo, N., Biggs, T. W., Castillo, C., Bingner, R. L., Langendoen, E. J., Taniguchi, K. T., Kretzschmar, T., Yuan, Y. P., & Liden, D. (2018). Measuring ephemeral gully erosion rates and topographical thresholds in an urban watershed using unmanned aerial systems and structure from motion photogrammetric techniques. *Land Degradation & Development, 29*(6), 1896-1905. doi:10.1002/ldr.2976

Harvey, A. M. (1992). Process interactions, temporal scales and the development of hillslope gully systems: Howgill Fells, northwest England. *Geomorphology, 5*(3-5), 323-344. doi:10.1016/0169-555x(92)90012-d

Hu, G., Wu, Y. Q., Liu, B. Y., Yu, Z. T., You, Z. M., & Zhang, Y. G. (2007). Short-term gully retreat rates over rolling hill areas in black soil of Northeast China. *Catena, 71*(2), 321-329. doi:10.1016/j.catena.2007.02.004

Kappler, C., Kaiser, K., Tanski, P., Klos, F., Fulling, A., Mrotzek, A., Sommer, M., & Bens, O. (2018). Stratigraphy and age of colluvial deposits indicating Late Holocene soil erosion in northeastern Germany. *Catena, 170*, 224-245. doi:10.1016/j.catena.2018.06.010

Kasielke, T., Poch, R. M., & Wiedner, K. (2019). Chernozem relics in the Hellweg Loess Belt (Westphalia, NW Germany) - Natural or man-made? *Quaternary International, 502*, 296-308. doi:10.1016/j.quaint.2018.09.015

Kasielke, T., & Zepp, H. (2011). Sediment fillings in valleys of the Ruhr area resulting from human impact in different periods of history. *Zeitschrift Fur Geomorphologie, 55*, 51-65. doi:10.1127/0372-8854/2011/0055s1-0037

Li, Z. W., Ning, K., Chen, J., Liu, C., Wang, D. Y., Nie, X. D., Hu, X. Q., Wang, L. X., & Wang, T. W. (2020). Soil and water conservation effects driven by the implementation of ecological restoration projects: Evidence from the red soil hilly region of China in the last three decades. *Journal of Cleaner Production, 260*, 13. doi:10.1016/j.jclepro.2020.121109

Liu, L., Chen, S., Sun, J. T., & Zhao, T. N. (2013). Analysis on the watershed features in hilly and gulliy loess area in west Shanxi. *Journal of Arid Land Resources & Environment, 27*(4), 146-152 (In Chinese with English abstract).

Liu, S., Cui, B., Zhang, Y., & Yang, X. K. (2020). Effects of topographical factors on erosion gully distribution of farmland in hilly areas of Jinlin Province. *Bulletin of Soil and Water Conservation, 40*(1), 38-42 (In Chinese with English abstract).

Liu, X., Burras, C. L., Kravchenko, Y. S., Duran, A., Huffman, T., Morras, H., Studdert, G., Zhang, X., Cruse, R. M., & Yuan, X. (2012). Overview of Mollisols in the world: Distribution, land use and management. *Canadian Journal of Soil Science, 92*(3), 383-402. doi:10.4141/Cjss2010-058

Liu, X., & Yan, B. (2009). Soil loss and food safety in Northeast China. Soil and Water Conservation in China. *Soil and Water Conservation in China*, (1), 17-19 (In Chinese with English abstract).

Liu, X., Zhang, S., Zhang, X., Ding, G., & Cruse, R. M. (2011). Soil erosion control practices in Northeast China: A mini-review. *Soil & Tillage Research, 117*, 44-48. doi:10.1016/j.still.2011.08.005

Ma, Q. H., Zhang, K. L., Jabro, J. D., Ren, L., & Liu, H. Y. (2019). Freeze–thaw cycles effects on soil physical properties under different degraded conditions in Northeast China. *Environmental Earth Sciences, 78*(10), 12. doi:10.1007/s12665-019-8323-z

Marzolff, I., & Poesen, J. (2009). The potential of 3D gully monitoring with GIS using high-resolution aerial photography and a digital photogrammetry system. *Geomorphology, 111*(1-2), 48-60. doi:10.1016/j.geomorph.2008.05.047

Mieth, A., & Bork, H. R. (2010). Humans, climate or introduced rats – which is to blame for the woodland destruction on prehistoric Rapa Nui (Easter Island)? *Journal of Archaeological Science, 37*(2), 417-426. doi:10.1016/j.jas.2009.10.006

Ministry of Water Resources, Chinese Academy of Sciences, & Engineering., C. A. O. (2010). *Soil erosion prevention and ecological security in China: The Black Soil Region in Northeast China*. Beijing: Science Press (In Chinese).

Moges, A., & Holden, N. M. (2008). Estimating the rate and consequences of gully development, a case study of Umbulo catchment in Southern Ethiopia. *Land Degradation & Development, 19*(5), 574-586. doi:10.1002/ldr.871

Nyssen, J., Poesen, J., Veyret-Picot, M., Moeyersons, J., Haile, M., Deckers, J., Dewit, J., Naudts, J., Teka, K., & Govers, G. (2006). Assessment of gully erosion rates through interviews and measurements: a case study from northern Ethiopia. *Earth Surface Processes and Landforms, 31*(2), 167-185. doi:10.1002/esp.1317

Owens, P. N., Walling, D. E., He, Q. P., Shanahan, J., & Foster, I. D. L. (1997). The use of caesium-137 measurements to establish a sediment budget for the Start catchment,

Devon, UK. *Hydrological Sciences Journal, 42*(3), 405-423. doi:10.1080/02626669709492037

Parsons, A. J., & Foster, I. D. L. (2011). What can we learn about soil erosion from the use of ^{137}Cs? *Earth-Science Reviews, 108*(1-2), 101-113. doi:10.1016/j.earscirev.2011.06.004

Poesen, J. (2018). Soil erosion in the Anthropocene: Research needs. *Earth Surface Processes and Landforms, 43*(1), 64-84. doi:10.1002/esp.4250

Poesen, J., Nachtergaele, J., Verstraeten, G., & Valentin, C. (2003). Gully erosion and environmental change: importance and research needs. *Catena, 50*(2-4), 91-133. doi:10.1016/S0341-8162(02)00143-1

Porto, P., & Walling, D. E. (2012). Validating the use of ^{137}Cs and ^{210}Pb$_{ex}$ measurements to estimate rates of soil loss from cultivated land in southern Italy. *Journal of Environmental Radioactivity, 106*, 47-57. doi:10.1016/j.jenvrad.2011.11.005

Soil Survey Staff. (2010). *Keys to soil taxonomy*. United States Department of Agriculture, Washington, D.C.: Government Printing Office.

Sun, J., & Liu, T. (2001). Desertification in the Northeastern China. *Quaternary Sciences, 21*(1), 72-78 (In Chinese with English abstract).

Sutherland, R. A. (1989). Quantification of accelerated soil erosion using the environmental tracer caesium-137. *Land Degradation and Development, 1*(3), 199-208. doi:10.1002/ldr.3400010304

Tarolli, P., Preti, F., & Romano, N. (2014). Terraced landscapes: From an old best practice to a potential hazard for soil degradation due to land abandonment. *Anthropocene, 6*, 10-25.

Tebebu, T. Y., Abiy, A. Z., Zegeye, A. D., Dahlke, H. E., Easton, Z. M., Tilahun, S. A., Collick, A. S., Kidnau, S., Moges, S., Dadgari, F., & Steenhuis, T. S. (2010). Surface

546 and subsurface flow effect on permanent gully formation and upland erosion near Lake
547 Tana in the northern highlands of Ethiopia. *Hydrology and Earth System Sciences, 14*(11), 2207-2217. doi:10.5194/hess-14-2207-2010
549 Vandekerckhove, L., Poesen, J., Wijdenes, D. O., & Gyssels, G. (2001). Short-term bank
550 gully retreat rates in Mediterranean environments. *Catena, 44*(2), 133-161.
551 doi:10.1016/S0341-8162(00)00152-1
552 Vanmaercke, M., Poesen, J., Van Mele, B., Demuzere, M., Bruynseels, A., Golosov, V.,
553 Bezerra, J. F. R., Bolysov, S., Dvinskih, A., Frankl, A., Fuseina, Y., Guerra, A. J. T.,
554 Haregeweyn, N., Ionita, I., Makanzu Imwangana, F., Moeyersons, J., Moshe, I., Nazari
555 Samani, A., Niacsu, L., Nyssen, J., Otsuki, Y., Radoane, M., Rysin, I., Ryzhov, Y. V.,
556 & Yermolaev, O. (2016). How fast do gully headcuts retreat? *Earth-Science Reviews, 154*, 336-355. doi:10.1016/j.earscirev.2016.01.009
558 Vattuone, M. S., Monne, J. L. P., Roldan, J., Maldonado, M., Lefebvre, M., & Vattuone,
559 M. (2018). Human-driven geomorphological processes and soil degradation in
560 Northwest Argentina: A geoarchaeological view. *Land Degradation & Development, 29*(11), 3852-3865. doi:10.1002/ldr.3128
562 Walling, D. E., & Quine, T. A. (1990). Calibration of caesium-137 measurements to provide
563 quantitative erosion rate data. *Land Degradation and Development, 2*(3), 161-175.
564 doi:10.1002/ldr.3400020302
565 Wen, Y., Kasielke, T., Li, H., Zhang, B., & Zepp, H. (2021). May agricultural terraces
566 induce gully erosion? A case study from the Black Soil Region of Northeast China.
567 *Science of the Total Environment, 750*, 141715. doi:10.1016/j.scitotenv.2020.141715
568 Wu, Y. Q., Zheng, Q. H., Zhang, Y. G., Liu, B. Y., Cheng, H., & Wang, Y. Z. (2008).
569 Development of gullies and sediment production in the black soil region of

northeastern China. *Geomorphology*, *101*(4), 683-691. doi:10.1016/j.geomorph.2008.03.008

Xu, J. Z., Li, H., Liu, X. B., Hu, W., Yang, Q. N., Hao, Y. F., Zhen, H. C., & Zhang, X. Y. (2019). Gully erosion induced by snowmelt in northeast china: A case study. *Sustainability*, *11*(7), 2088. doi:10.3390/su11072088

Xu, X. H., Sui, Y. Y., & Zhang, Y. (2014). Development of gully erosion and its influencing factors in hilly regions of Northeast China. *Acta Pedologica Sinica, 4*, 699-708 (In Chinese with English abstract).

Xu, Z., Qin, F., Zhang, B., Deng, Q., Liu, H., Jin, J., & Shi, L. (2018). The morphological characteristics of gully systems and watersheds in Dry-Hot Valley, SW China. *Acta Geochimica*, *37*(6), 854-866. doi:10.1007/s11631-018-0299-y

Yang, D., Xiong, D. H., Guo, M., Su, Z. G., Zhang, B. J., Zheng, X. Y., Zhang, S., & Fang, H. D. (2015). Impact of grass belt position on the hydraulic properties of runoff in gully beds in the Yuanmou Dry-hot valley region of Southwest China. *Physical Geography*, *36*(5), 408-425. doi:10.1080/02723646.2015.1074517

Yang, J. C., Zhang, S. W., Chang, L. P., Li, F., Li, T. Q., & Gao, Y. (2017). Gully erosion regionalization of black soil area in northeastern China. *Chinese Geographical Science, 27*(1), 78-87. doi:10.1007/s11769-017-0848-z

Ye, Y., & Fang, X. (2011). Spatial pattern of land cover changes across Northeast China over the past 300 years. *Journal of Historical Geography*, *37*(4), 408-417. doi:10.1016/j.jhg.2011.08.018

Zhang, X. C., Polyakov, V. O., Liu, B. Y., & Nearing, M. A. (2019). Quantifying geostatistical properties of ^{137}Cs and $^{210}Pb_{ex}$ at small scales for improving sampling design and soil erosion estimation. *Geoderma, 334*, 155-164. doi:10.1016/j.geoderma.2018.08.002

595 Zhang, X. C. J. (2015). New insights on using fallout radionuclides to estimate soil
596 redistribution rates. *Soil Science Society of America Journal, 79*(1), 1-8.
597 doi:10.2136/sssaj2014.06.0261
598 Zhang, Y., Zhao, Y. Y., Liu, B. Y., Wang, Z. Q., & Zhang, S. (2019). Rill and gully erosion
599 on unpaved roads under heavy rainfall in agricultural watersheds on China's Loess
600 Plateau. *Agriculture, Ecosystems & Environment, 284*, 106580.
601 doi:10.1016/j.agee.2019.106580
602 Zhang, Y. G., Wu, Y. Q., Lin, B. Y., Zheng, Q. H., & Yin, J. Y. (2007). Characteristics and
603 factors controlling the development of ephemeral gullies in cultivated catchments of
604 black soil region, Northeast China. *Soil & Tillage Research, 96*(1-2), 28-41.
605 doi:10.1016/j.still.2007.02.010
606 Zhang, Y. Q., Long, Y., Li, B., Xu, S. J., Wang, X. L., & Liao, J. (2017). Use of reservoir
607 deposits to reconstruct the recent changes in sediment yields from a small granite
608 catchment in the Yimeng Mountain region, China. *Geomorphology, 293*, 167-177.
609 doi:10.1016/j.geomorph.2017.05.017
610 Zhao, G. J., Mu, X. M., Wen, Z. M., Wang, F., & Gao, P. (2013). Soil erosion, conservation,
611 and eco-environment changes in the Loess Plateau of China. *Land Degradation &*
612 *Development, 24*(5), 499-510. doi:10.1002/ldr.2246
613

Figure Captions

Figure 1. Gully distribution map of the study area in 1968 (a) and 2018 (b). Gullies A-D used to measure gully volume using UAV in 2018 are marked.

Figure 2. Morphological changes of the Gullies A-D (Fig. 1) between 1968 and 2018.

Figure 3. (a) View from the head of Gully A over the partly afforested catchment. (b) Lower section of Gully C, showing the two parallel gully segments formed along former field cart roads. While the older gully on the right is inactive today, the left gully is actively eroding and had cut into the grey shales, causing collapsing of the gully walls (Photos: T. Kasielke).

Figure 4. Sketched soil profiles along the trench (a) and their positions at the outlet fan of Gully A (b) in comparison to a typical soil profile from the gully catchment not affected by gully erosion (c).

Figure 5. Distribution of ^{137}Cs in Bq kg^{-1} in selected soil profiles at the outlet fan of Gully A (cf. Fig. 4) and at a reference site. ^{137}Cs-samples are marked with an asterisk (*) to show zero values. For a complete legend, see Fig. 4.

Table 1. Gully lengths, gully density and forestland proportion within the 20 gully catchments of the study area.

Catchment No.	2018								Total gully length in 1968 (km)
	Area (km^2)	Total gully length (km)	Main gully length (km)	Total active gully length (km)	Total gully length in forestland (km)	Active gully length in forestland (km)	Gully density ($km\ km^{-2}$)	Forestland proportion† (%)	
1	0.91	3.8	1	3.3	3.2	2.9	4.2	22	2.1
2	0.11	0.3	0.1	0.3	0.3	0.3	2.7	55	0.4
3	0.4	2.4	0.5	2.1	1.5	1.5	6	22	1.2
4	0.99	1.1	0.4	0.8	1	0.7	1.1	55	2.4
5	0.06	0.2	0.1	0.2	0.2	0.2	3.3	69	0
6	0.25	0.9	0.3	0.8	0	0	3.6	19	0.2
7	1.18	3.2	1.4	3.2	2	2	2.7	18	2
8	0.51	1.1	0.2	0.9	0.7	0.5	2.2	15	0.3
9	0.21	0.6	0.2	0.6	0	0	2.9	5	0.1
10	1.89	4.6	1.6	3.2	2.5	1.5	2.4	12	1.6
11	0.26	0.6	0.4	0.5	0.1	0	2.3	18	0.3
12	0.29	1.2	0.3	1.1	0.8	0.8	4.1	27	0
13	2.65	9.8	2.3	9	5.4	4.8	3.7	7	6.9
14	1.02	0.9	0.3	0.7	0	0	0.9	0	0.2
15	0.98	1.4	0.3	1.4	0	0	1.4	10	0.9
16	1.18	3.8	1.6	3.8	3	3	3.2	6	0.9
17	0.83	1.7	0.6	1.5	1.1	0.5	2	5	1
18	0.57	1.5	0.6	0.8	1.7	0.6	2.6	4	0
19	1.76	2.7	1.7	2.7	0	0	1.5	0	1
20	4.01	4.9	2.5	4.9	0	0	1.2	0	2.5
Study area	20.06	46.7	16.4	41.8	23.5	19.3	2.3	11	24

†, estimated based on visual mapping of forestland (canopy cover is more than 10% and tree heights are more than 5 m) within each catchment and checked through field surveys

Table 2. Gully initiation years and erosion rates of Gullies A–D.

Gully	Gully initiation year calculated by Eq. 2 (approx. time reported by the farmers)	Gully volume 2018[†] (m^3)	Gully soil loss[‡] (Mg)	Gully drainage area[†] (ha)	Gully length 1968[§] (m)	Gully length 2018[†] (m)	Gully head retreat distance 1968-2018[§] (m)	Gully head retreat rate 1968-2018 ($m\ yr^{-1}$)	Gully area in 1968[§] (m^2)	Gully area in 2018[†] (m^2)	Gully area extension rate 1968-2018 ($m^2\ yr^{-1}$)	Gully soil loss rate[¶] ($m^3\ yr^{-1}$)	Gully soil loss rate per catchment area[※] ($m^3\ ha^{-1}\ yr^{-1}$)
A	~1955 (1950s)	93780	119101	43.9	379	547	155	2.5	22724	30962	165	1861	42.4
B	~1965 (1960s)	17045	21647	12.7	64	246	111	2.1	295	6726	129	401	31.6
C	~1966 (1960s)	10070	12789	5.4	87	300	117	2.3	186	5223	101	241	44.7
D	~1960 (1960s)	7630	9690	6.4	98	217	85	1.5	449.6	3273	57	164	25.7

[†], based on DSM of 2018.

[‡], calculated by gully volume and average soil bulk density of 1.27 Mg m^{-3}.

[§], estimated based on aerial photo from 1968 and/or satellite image from 2018.

[¶], gully volume divided the number of years since gully initiation.

[※], gully soil loss rate divided by the gully drainage area.

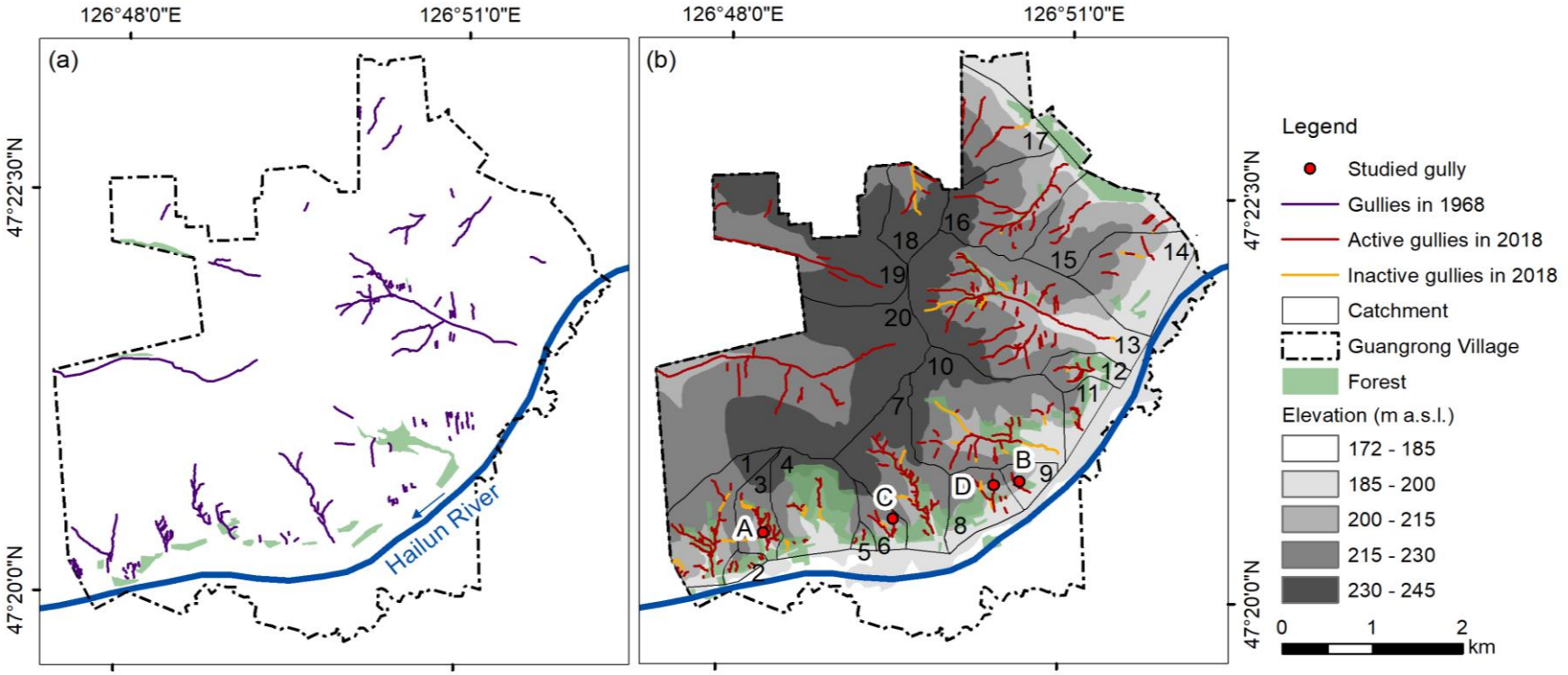

641

642 Fig. 1. Gully distribution map of the study area in 1968 (a) and 2018 (b). Gullies A-D used to measure gully volume using UAV in 2018 are
643 marked.

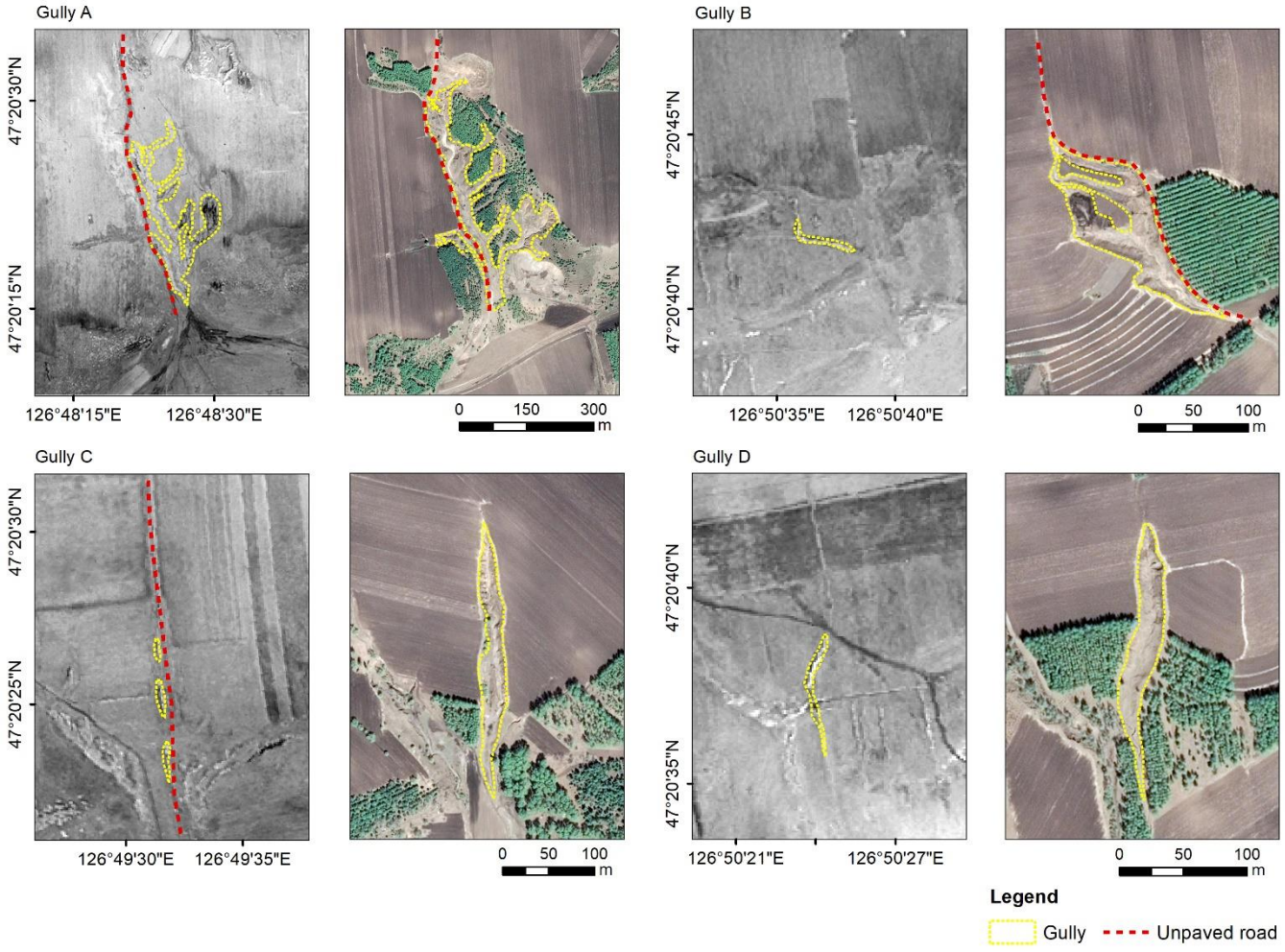

644

645 Fig. 2. Morphological changes of the Gullies A-D (Fig. 1) between 1968 and 2018.

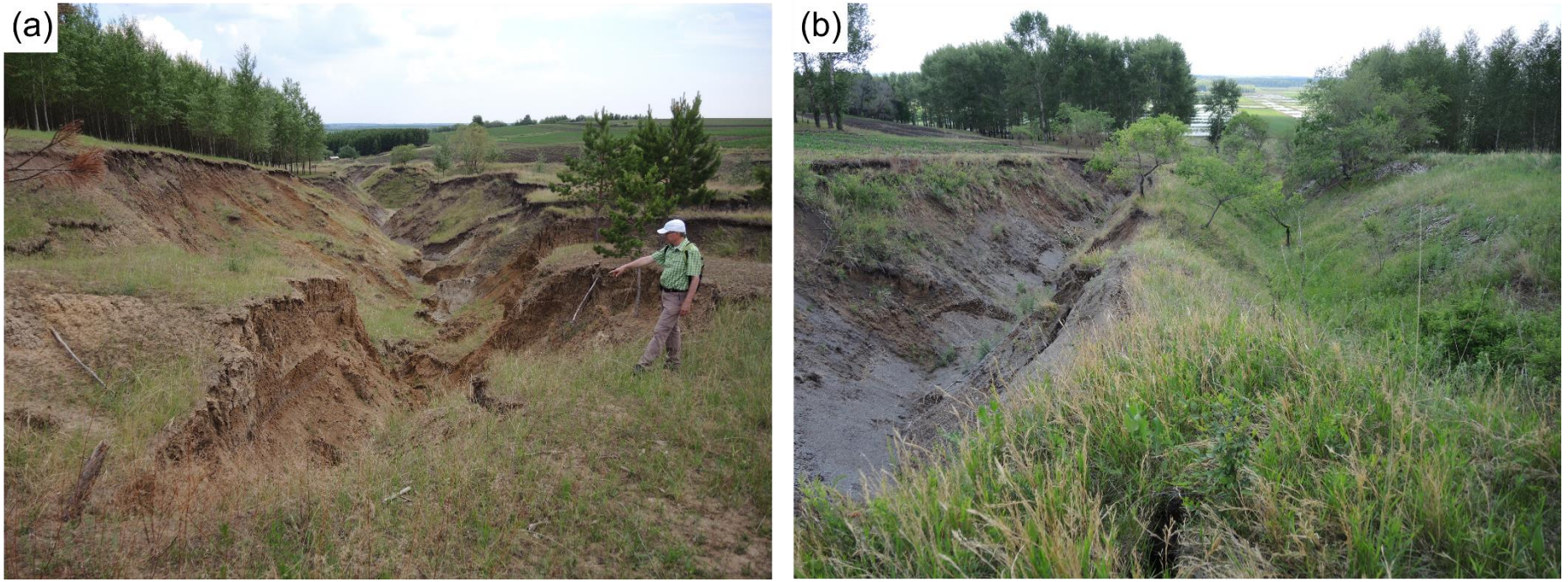

Fig. 3. (a) View from the head of Gully A over the partly afforested catchment. (b) Lower section of Gully C, showing the two parallel gully segments formed along former field cart roads. While the older gully on the right is inactive today, the left gully is actively eroding and had cut into the grey shales, causing slumping of the gully walls (Photos: T. Kasielke).

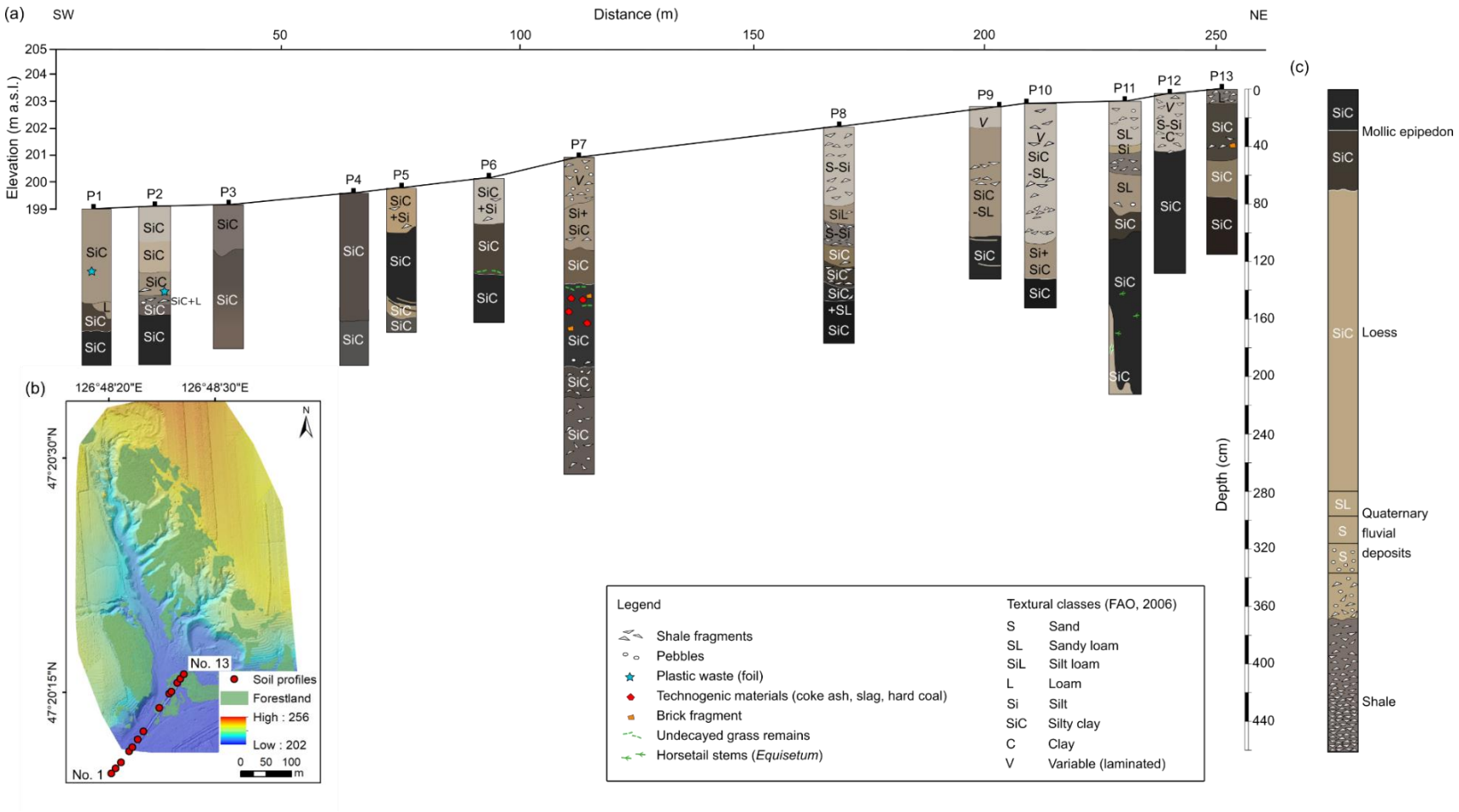

Fig. 4. Sketched soil profiles along the trench (a) and their positions at the outlet fan of Gully A (b) in comparison to a typical soil profile from the gully catchment not affected by gully erosion (c).

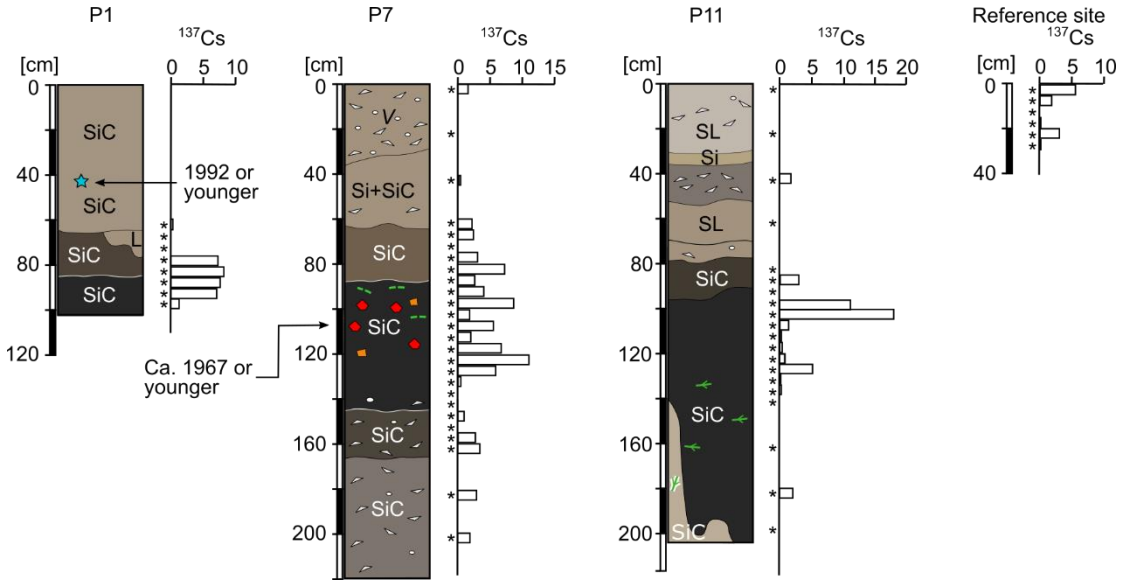

Fig. 5. Distribution of ^{137}Cs in Bq kg^{-1} in selected soil profiles at the outlet fan of Gully A (cf. Fig. 4) and at a reference site. ^{137}Cs-samples are marked with an asterisks (*) to show zero values. For a complete legend, the reader is referred to Fig. 4.